The Hydricity and Reactivity Relationship in [FeFe]-hydrogenases

Jacob Artz
NREL
David Mulder
Biosciences Center, National Renewable Energy Laboratory
Michael Ratzloff
NREL
John Peters
Washington State University
Paul King (Paul.King@nrel.gov)
National Renewable Energy Laboratory https://orcid.org/0000-0001-5039-654X

Article

Keywords: [FeFe]-hydrogenases, Hydricity, Reactivity, transition metal catalysts, enzymes

Posted Date: September 28th, 2020

DOI: https://doi.org/10.21203/rs.3.rs-77874/v1

Abstract

Reactivity of transition metal catalysts is controlled by covalent and non-covalent interactions that tune thermodynamic properties including hydricity. Hydricity is critical to catalytic activity and for modulating the reduction or oxidation of chemical compounds. Likewise, enzymes can employ transition metal cofactors and use metal-hydride intermediates tuned by protein frameworks to selectively control reactivity. One example, the [FeFe]-hydrogenases, catalyze reversible H_2 activation with H_2 oxidation to H^+ reduction ratios spanning ~10^7 in rate, offering a model to determine the extent that hydricity controls reactivity. To address this question, the hydricity of the catalytic H cluster of two [FeFe]-hydrogenases, CpI and CpII, were compared. We show that for CpI, the higher rates of H^+ reduction correspond to a more hydridic H cluster, whereas CpII, which strongly favors H_2 oxidation, has a less hydridic H cluster. The results demonstrate that enzymes manipulate metal cofactor hydricity to enable an extraordinary range of chemical reactivity.

Introduction

Metal-ligand complexes have fundamental roles in reduction-oxidation reactions, where covalent and non-covalent interactions strongly influence the metal-ligand reactivity.[1] One class of metal-ligand complexes, the transition metal hydrides, functions as intermediates in a broad number of chemical transformations.[2,3] For example, in small molecule activation reactions, hydricity of a catalytic metal site strongly influences the control of turnover rates and end-product specificities.[4] This effect of metal hydricity on a reduction-oxidation reaction is exemplified by control of H_2 reactivity in Ni-diphosphine complexes.[5] In these series of compounds, a more hydridic Ni-site strongly favors reduction of protons to form H_2, whereas weakly hydridic Ni sites favor H_2 binding and activation.[6] A caveat is that proton donor-acceptor p*K*a influences the reactivity trends, and matching of hydricity to p*K*a provides a means to further tune the end-product preferences of metal hydride based catalysts and their chemical reactions.[7,8]

Transition metals are critical to biological energy transformation reactions and are found in many enzyme active sites, including the FeMo cofactor in nitrogenase, leading to reduction of dinitrogen to ammonia,[9] the tungsten- or molybdenum-containing formate dehydrogenases, which reversibly reduce CO_2 to formate,[10] methyl coenzyme reductase,[11] which catalyzes the reduction of CH_3-S-CoM to methane, and hydrogenases, which catalyze reversible H_2 activation chemistry.[12,13] For the latter, striking differences in preferences for H_2 oxidation or H_2 production reactivity for a series of three unique [FeFe]-hydrogenases from *Clostridium pasteurianum* has been shown.[12,14] Each [FeFe]-hydrogenase incorporates a organometallic, iron-sulfur rich H cluster (Fig. 1), with additional iron-sulfur clusters, or F clusters, that can provide electron transfer functions.[15] The H cluster is composed of a [4Fe-4S] cubane linked by a protein cysteine thiolate ligand to a organometallic, diiron subsite ([2Fe]). The [2Fe] subsite has pairs of terminal CO and CN (*t*-CO and *t*-CN) ligands, a bridging CO (μ-CO) of the Fe atom pair, and a bridging azadithiolate ligand (Fig. 1).[16–19] The CO and CN ligands are critical for tuning the H cluster

electronic structure for heterolytic bond cleavage of H_2, where the μ-CO contributes a significant trans-effect for chemical H_2 activation at the distal Fe site (Fe_D) of [2Fe] subsite.[20,21] The residues surrounding the H cluster further modulate electronic structure,[22–24] electrostatics,[12] and redox potentials,[25] and observed differences in residue compositions may explain the reactivity variations among [FeFe]-hydrogenases. In support of this hypothesis, differences in the local H cluster electrostatics have been proposed to account for the variations in reactivity among the different *C. pasteurianum* [FeFe]-hydrogenases.[12]

Among the *C. pasteurianum* [FeFe]-hydrogenases, [FeFe]-hydrogenase II, or CpII, has a unique preference for H_2 oxidation, with a 10^4-fold higher reaction rate than proton reduction whereas *C. pasteurianum* [FeFe]-hydrogenase I, or CpI, has high rates of both proton reduction and H_2 oxidation, or more neutral reactivity.[12,26] The catalytic site of CpII also differs from CpI due to several changes in nearby non-covalent amino-acid interactions that are proposed to create a more hydrophobic environment around the catalytic site H cluster.[12] In this study, the biophysical properties of the CpII catalytic intermediates were compared to CpI in order to determine if there are underlying electronic properties that change H cluster thermodynamics to account for differences in reactivity. The outcomes clearly demonstrate that the CpII H cluster electronic structure is unique among [FeFe]-hydrogenases, and that the reactivity differences result from substantial changes in the H cluster hydricity that tune reactivity to favor H_2 oxidation.

Results And Discussion

CpII Resting State Electronic Structure. To identify possible differences in the electronic structure of the H cluster in CpII compared to other [FeFe]-hydrogenases, EPR and FTIR measurements were initially carried out on the well-characterized resting state of the enzyme, H_{ox}. For CpII, H_{ox} has a unique $S = 1/2$ EPR signal, with g-values of 2.08, 2.03, and 2.00 (Figure S1). However, the T_{opt} value was 40 K,[27] and higher than the T_{opt} average of 15 K for other [FeFe]-hydrogenases with differing reactivity profiles (Table S1). The difference in the relaxation property of the signal suggests that the H cluster in CpII has more [2Fe-2S] cluster character[28] compared to [FeFe]-hydrogenases with more neutral reactivity such as CpI, suggesting that CpII may have subtle differences in its electronic structure or distribution of spin on [2Fe].[22] The corresponding FTIR spectra (Fig. 2) of the resting state CpII (H_{ox}) has νCN bands at 2082 and 2069 cm^{-1}, and terminal νCO bands at 1969 and 1944 cm^{-1}, however the νCO band of the μ-CO that bridges the diiron sub-site Fe atoms was at 1752 cm^{-1}, or ~ 50 cm^{-1} downshifted compared to the FTIR spectra of H_{ox} for CpI (Table 1) and other [FeFe]-hydrogenases (Table S2). This signifies an increase of π back-bonding from $Fe_D \rightarrow \mu$-CO in CpII, which is further illustrated by the differences in the FTIR spectrum of H_{ox} sample treated with CO (H_{ox}-CO). CO is a π-acceptor ligand that terminally binds at the ligand exchangeable site of the Fe_D atom (Fig. 1).[21] For CpII, the H_{ox}-CO form has an exogenous νCO band at 2023 cm^{-1}, which is upshifted by 6 cm^{-1} relative to same band at 2017 cm^{-1} in CpI H_{ox}-CO (Fig. 2, Table 1). Thus, the downshift of μ-CO frequency in CpII (greater π back-bonding from Fe_D into μ-CO)

compared to CpI is also matched by an upshift in *t*-CO frequency (less π back-bonding from Fe_D into *t*-CO) in CpII relative to CpI (Table 1), owing to differences in the underlying H cluster electronic structures between the two enzymes. Collectively, the EPR and FTIR properties of resting state CpII indicate differences in electronic structure compared to CpI, which is likely to affect the properties of catalytic intermediates.

Table 1
The *v*CO of the H_{ox} and H_{ox}-CO states.

Enzyme	State	Terminal *v*CO	Δ*v*CO
CpI[a]	H_{ox}	1971, 1948	23
CpII	H_{ox}	1969, 1944	25
$CpII^{C\rightarrow S}$	H_{ox}	1973, 1950	23
CpI[a]	H_{ox}-CO	2017, 1974, 1971	43, 3
CpII	H_{ox}-CO	2023, 1975, 1960	48, 15

[a] values for CpI.[56]

Properties of the Reduced Intermediates of CpII. Redox poising of [FeFe]-hydrogenases at defined potentials in combination with EPR and FTIR spectroscopy can identify the spectral signatures of catalytic intermediates that arise from changes in the H cluster oxidation state and electronic structure.[29–32] Each of the H cluster intermediates in Fig. 1 has a distinctive EPR and FTIR signal, for example, the reduction of H_{ox} by 1-electron leads to formation of H_{red}, and a second reduction step leads to formation of either H_{sred}, or H_{hyd} that has a terminally bound hydride. Poising samples can be used to identify and determine the relative populations of the 2-electron reduced intermediates, H_{sred} and H_{hyd}, and thus inform on the hydricity of the H cluster.[33]

When poised under reducing conditions, the EPR spectrum of CpII is composed of two signals, a fast-relaxing signal (g = 2.070, 1.936, 1.867) with a T_{opt} of 5 K, which can be assigned to H_{sred},[34,35] and an additional rhombic signal (g = 2.058, 1.92, 1.89) with a T_{opt} of 15 K, which can be assigned to the reduced, paramagnetic F clusters (Figure S2, Table S3).[26] As potentials became more negative, CpII formed only H_{sred}, and there was no equivalent H_{hyd} signal[29,36] even at potentials as low as -625 mV (Figure S2). The addition of the natural substrate, H_2 and poising at -490 mV, led to higher enrichments of H_{sred} (Table S3), which is a result of H_2 oxidation. Nonetheless, the addition of H_2 also failed to lead to a detectable formation of the hydride intermediate, H_{hyd}, EPR signal originating from a reduced [4Fe-4S] subsite (Fig. 1).[29]

The corresponding FTIR spectra of CpII were measured as it is possible to observe a more complete profile of the reduced state populations due to all the reduced states having unique IR spectral signatures (Table S2). This is evident as collective downshifts of *t*-CO bands for both the H_{red} and H_{sred} states compared to H_{ox} (Fig. 2) owing to the formal reduction of the H cluster subsites.[37,38] Under the reducing potentials used here, the H cluster of CpII predominantly equilibrates into the 1-electron reduced H_{red} state, with a smaller population of the 2-electron reduced H_{sred} state being observed at -625 mV (Fig. 3A), consistent with the EPR results (Table S3). A spectral feature of the H cluster hydride intermediate, H_{hyd}, in [FeFe]-hydrogenases is the presence of a μ-CO band at ~ 1850–1870 cm^{-1},[29,36,39–41] which arises from a terminally bound hydride at the open coordination site of Fe_D of the [2Fe] subsite. This feature was not detected in the FTIR spectra of CpII poised at reducing potentials (Fig. 3A), consistent with the EPR results from Figure S2, Table S3.

CpII $^{C \rightarrow S}$ Traps the 2-electron Reduced Intermediate of CpII. A strictly conserved cysteine residue in [FeFe]-hydrogenase that is proximal to the H cluster, forms a part of the proton-transfer relay to the active-site. When the cysteine is changed to a serine (C→S) this exchanges a -SH for a -OH, which disrupts proton-transfer and traps the enrichment of the 2-electron reduced state in [FeFe]-hydrogenases.[29] For neutral bias enzymes this results in a pronounced enrichment of the H_{hyd} state.[29,41] Thus, a C→S variation of the proton-relay can reveal the preferred 2-electron reduced state, and directly inform on whether the hydricity of the H cluster changes in enzymes that have different catalytic site microenvironments.

The effect of the C→S variation on CpII was determined under redox poising (Fig. 3) and compared to CpII. At the less reducing potential of -375 mV, $CpII^{C \rightarrow S}$ is primarily poised in the 1-electron reduced state H_{red} with *t*-CO bands at 1901 and 1882 cm^{-1} consistent with the addition of electron density to the [$2Fe_H$] compared to the resting state spectrum (Fig. 3). Further reduction of $CpII^{C \rightarrow S}$ to more reducing potentials led to a more enriched formation of H_{sred} compared to CpII (Fig. 3A).[38] Likewise, the corresponding EPR spectra recorded at 5 K showed an overall weak signal that increased in intensity at lower reduction potentials due to the increased presence of both H_{sred} [34,35] and reduced F clusters (Fig. 3B, Figure S3, Table S3).[27] Overall, the 1906 and 1872 cm^{-1} *t*-CO bands in $CpII^{C \rightarrow S}$ are consistent with assignment to the 2-electron reduced H_{sred} intermediate, which matches to a weaker H_{sred} *t*-CO band at 1879 cm^{-1} in CpII poised at -625 mV. Thus, in contrast to what has been observed for neutral bias [FeFe]-hydrogenases, the C→S variation leads to enrichment of H_{sred} in CpII, supported by a lack of H_{hyd} in any of the reduced or H_2 treated samples.

H/D Isotope Editing of Reduced CpII. In order to further corroborate that the preferred 2-electron reduced intermediate of CpII is H_{sred} rather than H_{hyd}, H/D isotope experiments were carried out under H_2 or D_2 gas. H/D isotope-editing combined with FTIR spectroscopy of [FeFe]-hydrogenases has been used to identify the H_{hyd} intermediate, which is observed as a H→D isotope induced shift of the μ-CO IR band due to the trans-effect of the terminally bound hydride on the adjacent Fe_D atom (Fig. 1).[38,39] Treatment of

CpII with either H_2 (H_2O) or D_2 (D_2O) (Fig. 4) led to a downshift of the *v*CO bands owing to binding and activation of H_2 or D_2 accompanied by reduction of the resting state H cluster (Fig. 1). The FTIR spectra indicate CpII is mainly poised in the H_{red} state with terminal *v*CO at 1918 and 1889 cm^{-1}, and a μ-CO band at 1730 cm^{-1}, with a smaller population of H_{sred} (Fig. 4, top panel). A clear lack of an H/D isotope sensitive μ-CO band, the defining feature of the H_{hyd} spectrum[36] (Table S2), strongly supports that the H cluster of CpII is tuned to favor H_{sred} in the 2-electron reduced state over H_{hyd}, and again consistent with enrichment of H_{sred} in $CpII^{C\rightarrow S}$. Due to the lack of an observable "H_{hyd}" state, the H/D exchange activity of CpII was measured in order to determine whether the catalytic mechanism involves heterolytic H_2 activation.[42] In reactions under H_2 in D_2O, purified CpII co-evolved both HD and D_2, (Figure S4), confirming the catalytic mechanism of CpII involves formation of a H_{hyd} state, which due to low hydricity favors H_2 oxidation (Figure S5).

$CpII^{C\rightarrow S}$ Reactivity has Increased Bias Towards H_2 oxidation. The spectroscopic properties of $CpII^{C\rightarrow S}$ demonstrate a change in the proton relay that leads to a greater stabilization of $H_{sred,}$ compared to CpII. Based on the observed scaling relationship between H cluster hydricity and enzymatic reactivity in CpII versus CpI, where H_2 oxidation rates are favored by a less hydridic H cluster, the reactivity of $CpII^{C\rightarrow S}$ is predicted to further shift towards H_2 oxidation compared to CpII. The reactivity ratio of $CpII^{C\rightarrow S}$ for H_2 oxidation-to-proton reduction is 10^4 versus 10^3 for CpII (Table S4), a difference of 10-fold in favor of H_2 oxidation. Thus, a change in the hydricity of the H cluster leads to more favorable formation of H_{sred} over H_{hyd} and favors H_2 oxidation over proton reduction. This effect is accentuated for CpII by a shift in the p*K*a landscape of proton transfer, where the electronic structure leads to a more acidic Fe_D relative to the proton relay Cys residue (see Fig. 1). This difference is further magnified in $CpII^{C\rightarrow S}$ where -SH to -OH creates an even larger difference in the p*K*a between the proton donor and hydride binding sites.

Conclusions

Redox enzymes exhibit broad preferences for catalyzing the reduction or oxidation of a chemical substrate. For hydrogenases, several mechanisms have been proposed to account for differences reversibility of H_2 activation as a preference for H^+ reduction or H_2 oxidation. Due to the fact that hydrogenases share a common catalytic site cofactor and use similar redox intermediates, reactivity differences have been mainly attributed to differences in accessory clusters[43–45] and extended proton transfer pathways.[46–49]

A less obvious property of enzymes that is known to profoundly affect reactivity of transition metal complexes is the thermodynamic hydricity. The understanding of hydricity and reactivity is embodied in scaling relationships that directly account for observed rate differences of reduction-oxidation reactions. Model compounds control broad reactivity ranges using primary and secondary sphere chemistry.[5,33] This relationship is exemplified for CpI and CpII in Fig. 5 where the dramatic difference in reactivity is a

direct outcome of the thermodynamic hydricity. This result now explains why manipulation of [FeFe]-hydrogenase catalytic site microenvironments[29,36] can be modeled as changes in hydricity by computational analysis.[33]

What these studies reveal is that tuning of the H cluster hydricity and p*K*a regimes provides for kinetic control over reactive intermediates in the heterolytic exchange of H_2, H^+, and electrons (Figure S5).[50] The H cluster microenvironment in CpI, and likewise for other neutral bias [FeFe]-hydrogenases, favors more reversible equilibrium of reduced states like H_{hyd}[29,38] and H_{sred}. In contrast, this work reveals that the modulation of the H cluster electronic structure in CpII leads to changes in the pK_a landscape for protonation-deprotonation of Fe_D. This effect manifests as differences in the acidity of the Fe_D site on the H cluster (i.e., a lower μ-CO frequency (50–70 cm^{-1}, Table S2) for all oxidation states due to greater back-bonding from Fe_D.[21,51,52] As a result, the Fe_D site is more acidic, and protonation of the reduced H cluster is strongly disfavored in CpII, an effect which is strengthened in $CpII^{C\rightarrow S}$. In CpII, the outcome is a significantly less stable H_{hyd} state and kinetic equilibrium favoring H_{red} and H_{sred} and H_2 oxidation.

The organic framework of Ni-phosphines, diiron-organometallic complexes have been extensively modified to understand how hydricity, p*K*a, and redox potential of metal sites determine catalytic properties.[53–55] Metal site sterics, solvation networks, electronic structure, hydrogen bonding and electrostatics contribute to the hydricity, by scaling relationships. It is possible that the subtle changes in the H cluster microenvironment of CpII versus CpI exacts a similar range of control. Model complexes have an additional layer of control through changing the solvent system or using rare-earth metals. However, the broad range of reactivities in [FeFe]-hydrogenases demonstrates that reactivity may be sufficiently tuned using earth-abundant materials and aqueous solvent.

Summary

We have conducted a thorough analysis of the catalytic site electronic structure and relationship to the H_2 activation mechanism of [FeFe]-hydrogenase CpII. These changes underlie and determine the hydricity to favor the formal 2-electron reduced catalytic site (lower hydricity) over a hydride bound intermediate, and reactivity towards H_2 oxidation. Changing the proton-donor amino acid from acidic to basic, further shifts reactivity towards H_2 oxidation by introducing a barrier to protonation of the hydride bound H cluster. These changes are likely elicited by subtle differences in the amino acids that comprise the microenvironment of catalytic site H cluster, establishing a template for how the natural chemistry of redox enzymes can be utilized to optimize organometallic site reactivity. It may also make possible the implementation of rational design to reengineer redox enzymes and their reactivities for optimized production of desired compounds.

Declarations

Acknowledgements. This work is supported as part of the Biological and Electron Transfer and Catalysis (BETCy) EFRC, an Energy Frontier Research Center funded by the U.S. Department of Energy, Office of Science (DE-SC0012518) (JA, DM, MR, JP and PK), and the Basic Energy Sciences, Chemical Sciences, Geosciences and Biosciences Division, Photosynthetic Systems Program (JA, DM and PK). This work was authored by Alliance for Sustainable Energy, LLC, the manager and operator of the National Renewable Energy Laboratory for the U.S. Department of Energy (DOE) under Contract No. DE-AC36-8GO28308. The views expressed in the article do not necessarily represent the views of the DOE or the U.S. Government. The U.S. Government and the publisher, by accepting the article for publication, acknowledges that the U.S. Government retains a nonexclusive, paid-up, irrevocable, worldwide license to publish or reproduce the published form of this work, or allow others to do so, for U.S. Government purposes.

Author Contributions. J.H.A. performed protein purification and activity measurements. J.H.A. and D.W.M. performed spectroscopic analyses. P.W.K. performed H/D exchange measurements. All authors contributed to the design of the study, interpreting experimental results, and writing the manuscript.

Competing Interests. The authors declare no competing interests.

References

1. Oswald, V. F. *et al.* Effects of Noncovalent Interactions on High-Spin Fe(IV)–Oxido Complexes. *J. Am. Chem. Soc.* **142**, 11804–11817, (2020).
2. Craig, P., Crabtree, R.H. *The Organometallic Chemistry of the Transition Metals, 5th edn* (John Wiley and Sons, 2009)
3. Heinekey, D. M. & Oldham, W. J. Coordination Chemistry of Dihydrogen. *Chem. Rev.* **93**, 913–926, (1993).
4. Kubas, G. J. *Metal Dihydrogen and s-Bond Complexes: Structure, Theory, and Reactivity*. (Springer US, 2001).
5. DuBois, M. R. & DuBois, D. L. The Roles of the First and Second Coordination Spheres in the Design of Molecular Catalysts for H_2 production and Oxidation. *Chem. Soc. Rev.* **38**, 62–72, (2009).
6. Raugei, S. *et al.* Experimental and Computational Mechanistic Studies Guiding the Rational Design of Molecular Electrocatalysts for Production and Oxidation of Hydrogen. *Inorg. Chem.* **55**, 445–460, (2016).
7. Wiedner, E. S. *et al.* Thermodynamic Hydricity of Transition Metal Hydrides. *Chem. Rev.* **116**, 8655–8692, (2016).
8. Tsay, C., Livesay, B. N., Ruelas, S. & Yang, J. Y. Solvation Effects on Transition Metal Hydricity. *J. Am. Chem. Soc.* **137**, 14114–14121, (2015).
9. Yang, Z.-Y. *et al.* On Reversible H_2 Loss Upon N_2 Binding to FeMo-cofactor of Nitrogenase. *Proc. Natl. Acad. Sci.* **110**, 16327–16332, (2013).

10. Yu, X., Niks, D., Mulchandani, A. & Hille, R. Efficient Reduction of CO_2 by the Molybdenum-Containing Formate Dehydrogenase from *Cupriavidus necator* (*Ralstonia eutropha*). *J. Biol. Chem.* **292**, 16872–16879, (2017).
11. Harmer, J. *et al.* A Nickel Hydride Complex in the Active Site of Methyl-Coenzyme M Reductase: Implications for the Catalytic Cycle. *J. Am. Chem. Soc.* **130**, 10907–10920, (2008).
12. Artz, J. H. *et al.* Tuning Catalytic Bias of Hydrogen Gas Producing Hydrogenases. *J. Am. Chem. Soc.* **142**, 1227–1235, (2020).
13. Schilter, D., Camara, J. M., Huynh, M. T., Hammes-Schiffer, S. & Rauchfuss, T. B. Hydrogenase Enzymes and Their Synthetic Models: The Role of Metal Hydrides. *Chem. Rev.* **116**, 8693–8749, (2016).
14. Adams, M. W., Eccleston, E. & Howard, J. B. Iron-sulfur Clusters of Hydrogenase I and Hydrogenase II of *Clostridium pasteurianum*. *Proc. Natl. Acad. Sci. U.S.A.* **86**, 4932–4936, (1989).
15. Vignais, P. M. & Billoud, B. Occurrence, Classification, and Biological Function of Hydrogenases: An Overview. *Chem. Rev.* **107**, 4206–4272, (2007).
16. Peters, J. W., Lanzilotta, W. N., Lemon, B. J. & Seefeldt, L. C. X-ray Crystal Structure of the Fe-only Hydrogenase (CpI) from *Clostridium pasteurianum* to 1.8 Angstrom Resolution. *Science* **282**, 1853–1858 (1998).
17. Nicolet, Y., Piras, C., Legrand, P., Hatchikian, C. E. & Fontecilla-Camps, J. C. *Desulfovibrio desulfuricans* Iron Hydrogenase: the Structure Shows Unusual Coordination to an Active Site Fe Binuclear Center. *Structure* **7**, 13–23, (1999).
18. Silakov, A., Wenk, B., Reijerse, E. & Lubitz, W. 14 N HYSCORE Investigation of the H-cluster of [FeFe] hydrogenase: Evidence for a Nitrogen in the Dithiol Bridge. *Phys. Chem. Chem. Phys.* **11**, 6592–6599, (2009).
19. Berggren, G. *et al.* Biomimetic Assembly and Activation of [FeFe]-hydrogenases. *Nature* **499**, 66–69, (2013).
20. Kubas, G. J. Fundamentals of H_2 Binding and Reactivity on Transition Metals Underlying Hydrogenase Function and H_2 Production and Storage. *Chem. Rev.* **107**, 4152–4205, (2007).
21. Lemon, B. J. & Peters, J. W. Photochemistry at the Active Site of the Carbon Monoxide Inhibited form of the Iron-only Hydrogenase (CpI). *J. Am. Chem. Soc.* **122**, 3793–3794, (2000).
22. Popescu, C. V. & Münck, E. Electronic Structure of the H Cluster in [Fe]-Hydrogenases. *J. Am. Chem. Soc.* **121**, 7877–7884, (1999).
23. Lampret, O. *et al.* Interplay between CN– Ligands and the Secondary Coordination Sphere of the H-Cluster in [FeFe]-Hydrogenases. *J. Am. Chem. Soc.* **139**, 18222–18230, (2017).
24. Knorzer, P. *et al.* Importance of the Protein Framework for Catalytic Activity of [FeFe]-Hydrogenases. *J. Biol. Chem.* **287**, 1489–1499, (2011).
25. Rodríguez-Maciá, P. *et al.* His-Ligation to the [4Fe–4S] Subcluster Tunes the Catalytic Bias of [FeFe] Hydrogenase. *J. Am. Chem. Soc.* **141**, 472–481, (2019).

26. Adams, M. W. & Mortenson, L. E. The Physical and Catalytic Properties of Hydrogenase II of *Clostridium pasteurianum*. A comparison with Hydrogenase I. *J. Biol. Chem.* **259**, 7045–7055 (1984).
27. Adams, M. W. The Mechanisms of H_2 Activation and CO Binding by Hydrogenase I and Hydrogenase II of *Clostridium pasteurianum*. *J. Biol. Chem.* **262**, 15054–15061 (1987).
28. Cammack, R. & MacMillan, F. in *Metals in Biology: Applications of High-Resolution EPR to Metalloenzymes* (Springer New York, 2010).
29. Mulder, D. W., Guo, Y., Ratzloff, M. W. & King, P. W. Identification of a Catalytic Iron-hydride at the H-cluster of [FeFe]-hydrogenase. *J. Am. Chem. Soc.* **139**, 83–86, (2017).
30. Sommer, C. *et al.* Proton Coupled Electronic Rearrangement within the H-Cluster as an Essential Step in the Catalytic Cycle of [FeFe] Hydrogenases. *J. Am. Chem. Soc.* **139**, 1440–1443, (2017).
31. Lubitz, W., Ogata, H., Rüdiger, O. & Reijerse, E. Hydrogenases. *Chem. Rev.* **114**, 4081–4148, (2014).
32. Land, H., Senger, M., Berggren, G. & Stripp, S. T. Current State of [FeFe]-Hydrogenase Research: Biodiversity and Spectroscopic Investigations. *ACS Catal.* **10**, 7069–7086, (2020).
33. Wiedner, E. S. Thermodynamic Hydricity of [FeFe]-Hydrogenases. *J. Am. Chem. Soc.* **141**, 7212–7222, (2019).
34. Agnieszka, A. *et al.* Identification and Characterization of the “Super-Reduced” State of the H-Cluster in [FeFe] Hydrogenase: A New Building Block for the Catalytic Cycle? *Angew. Chem. Int. Ed.* **51**, 11458–11462, (2012).
35. Mulder, D. W. *et al.* EPR and FTIR Analysis of the Mechanism of H_2 Activation by [FeFe]-Hydrogenase HydA1 from *Chlamydomonas reinhardtii*. *J. Am. Chem. Soc.* **135**, 6921–6929, (2013).
36. Mulder, D. W. *et al.* Investigations on the Role of Proton-Coupled Electron Transfer in Hydrogen Activation by [FeFe]-Hydrogenase. *J. Am. Chem. Soc.* **136**, 15394–15402, (2014).
37. Birrell, J. A. *et al.* Spectroscopic and Computational Evidence that [FeFe] Hydrogenases Operate Exclusively with CO-Bridged Intermediates. *J. Am. Chem. Soc.* **142**, 222–232, (2020).
38. Ratzloff, M. W. *et al.* CO-Bridged H-Cluster Intermediates in the Catalytic Mechanism of [FeFe]-Hydrogenase CaI. *J. Am. Chem. Soc.* **140**, 7623–7628, (2018).
39. Pham, C. C. *et al.* Terminal hydride species in [FeFe]-hydrogenases are Vibrationally Coupled to the Active Site Environment. *Angew. Chem. Int. Ed.* **130**, 10765–10769, (2018).
40. Reijerse, E. J. *et al.* Direct Observation of an Iron-Bound Terminal Hydride in [FeFe]-Hydrogenase by Nuclear Resonance Vibrational Spectroscopy. *J. Am. Chem. Soc.* **139**, 4306–4309, (2017).
41. Winkler, M. *et al.* Accumulating the Hydride State in the Catalytic Cycle of [FeFe]-hydrogenases. *Nat. Commun.* **8**, 16115, (2017).
42. Fauque, G. D. *et al.* A Proton-Deuterium Exchange Study of Three Types of *Desulfovibrio* Hydrogenases. *J. Ind. Microbio.* **2**, 15–23 (1987).
43. Rodríguez-Maciá, P. *et al.* Intercluster Redox Coupling Influences Protonation at the H-cluster in [FeFe] Hydrogenases. *J. Am. Chem. Soc.* **139**, 15122–15134, (2017).

44. Caserta, G. *et al.* Engineering an [FeFe]-Hydrogenase: Do Accessory Clusters Influence O_2 Resistance and Catalytic Bias? *J. Am. Chem. Soc.* **140**, 5516–5526, (2018).
45. Hexter, S. V., Grey, F., Happe, T., Climent, V. & Armstrong, F. A. Electrocatalytic Mechanism of Reversible Hydrogen Cycling by Enzymes and Distinctions Between the Major Classes of hydrogenases. *Proc. Natl. Acad. Sci.* **109**, 11516–11521 (2012).
46. Lampret, O. *et al.* The Roles of Long-range Proton-Coupled Electron Transfer in the Directionality and Efficiency of [FeFe]-hydrogenases. *Proc. Natl. Acad. Sci* **117**, 20520–20529, (2020).
47. Ginovska-Pangovska, B. *et al.* Molecular Dynamics Study of the Proposed Proton Transport Pathways in [FeFe]-hydrogenase. *Biochim.Biophys. Acta, Bioenerg.* **1837**, 131–138, (2014).
48. Cornish, A. J., Gartner, K., Yang, H., Peters, J. W. & Hegg, E. L. Mechanism of Proton Transfer in [FeFe]-Hydrogenase from *Clostridium pasteurianum*. *J. Biol. Chem.* **286**, 38341–38347, (2011).
49. Cornish, A. J. *et al.* Single-Amino Acid Modifications reveal Additional Controls on the Proton Pathway of [FeFe]-Hydrogenase. *Biochemistry* **55**, 3165–3173, (2016).
50. Huhmann-Vincent, J., Scott, B. L. & Kubas, G. J. Reactions of H_2, Silanes, and Olefins with Superelectrophilic Cationic Rhenium Complexes: Heterolytic Cleavage of H_2 and Relation to the Structure and Function of Hydrogenases. *Inorg. Chim. Acta* **294**, 240–254, (1999).
51. Nicolet, Y. *et al.* Crystallographic and FTIR Spectroscopic Evidence of Changes in Fe Coordination Upon Reduction of the Active Site of the Fe-Only Hydrogenase from *Desulfovibrio desulfuricans*. *J. Am. Chem. Soc.* **123**, 1596–1601, (2001).
52. Lemon, B. J. & Peters, J. W. Binding of Exogenously Added Carbon Monoxide at the Active Site of the Iron-Only Hydrogenase (CpI) from *Clostridium pasteurianum*. *Biochemistry* **38**, 12969–12973, (1999).
53. Ellis, W. W., Miedaner, A., Curtis, C. J., Gibson, D. H. & DuBois, D. L. Hydride Donor Abilities and Bond Dissociation Free Energies of Transition Metal Formyl Complexes. *J. Am. Chem. Soc.* **124**, 1926–1932, (2002).
54. Rauchfuss, T. B. Diiron Azadithiolates as Models for the [FeFe]-Hydrogenase Active Site and Paradigm for the Role of the Second Coordination Sphere. *Acc. Chem. Res.* **48**, 2107–2116, (2015).
55. Camara, J. M. & Rauchfuss, T. B. Combining Acid–Base, Redox and Substrate Binding Functionalities to Give a Complete Model for the [FeFe]-hydrogenase. *Nat. Chem.* **4**, 26–30, (2012).
56. Chen, Z. *et al.* Infrared Studies of the CO-Inhibited Form of the Fe-Only Hydrogenase from *Clostridium pasteurianum* I: Examination of Its Light Sensitivity at Cryogenic Temperatures. *Biochemistry* **41**, 2036–2043, (2002).

Figures

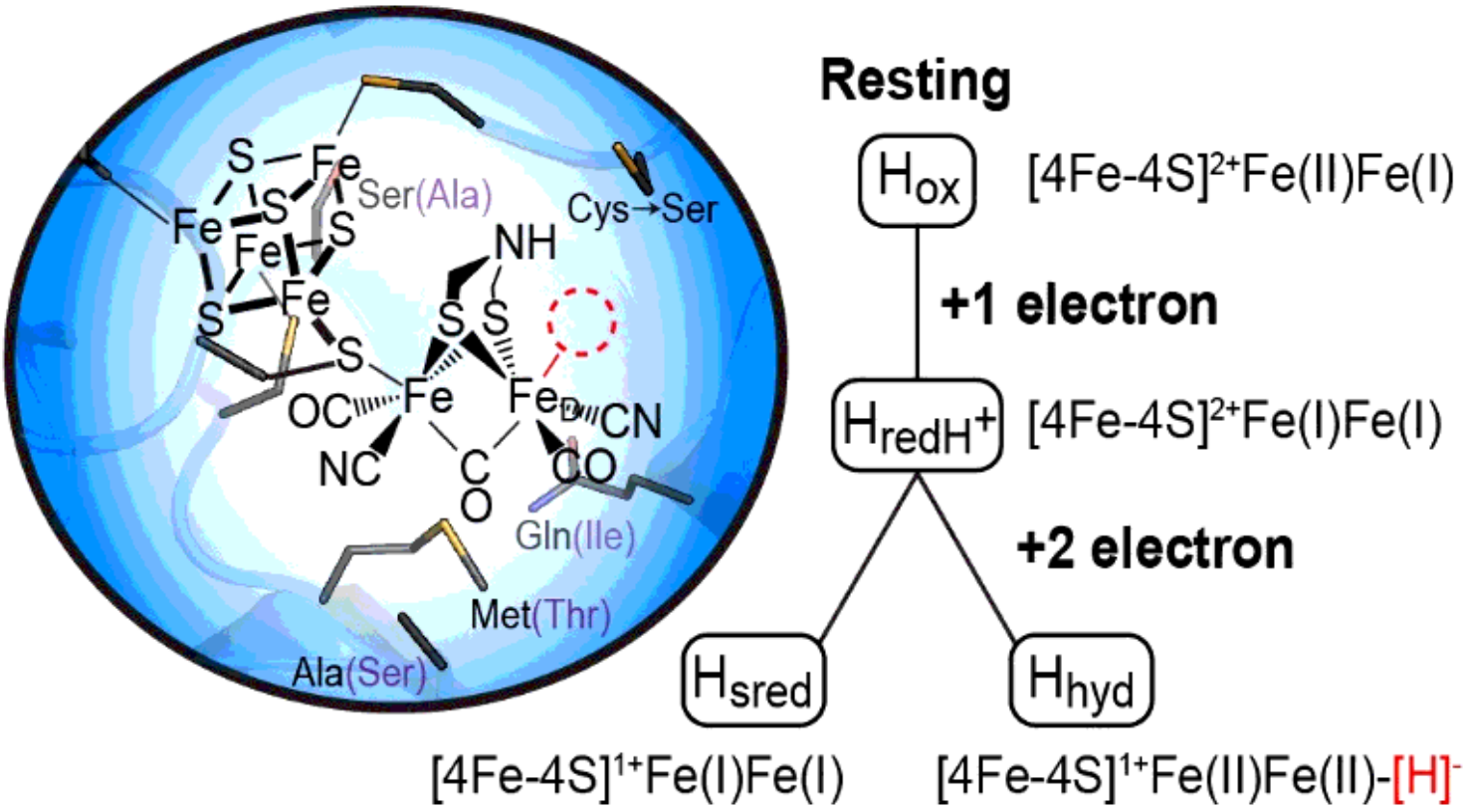

Figure 1

The [FeFe]-hydrogenase H cluster Microenvironment and Defined Redox States. On the left, the non-covalent amino acids nearby the H cluster, consisting of a [4Fe-4S] subsite and [2Fe] organometallic subsite, that differ between CpI (black, Ala230, Cys299, Gln325, Met353) and CpII (purple, Ser99, Cys169, Ile195, Thr223) are shown. The hydride-coordinating, exchangeable site on FeD is outlined in a red-dashed circle. On the right, the formal electronic structures of the H cluster redox states.

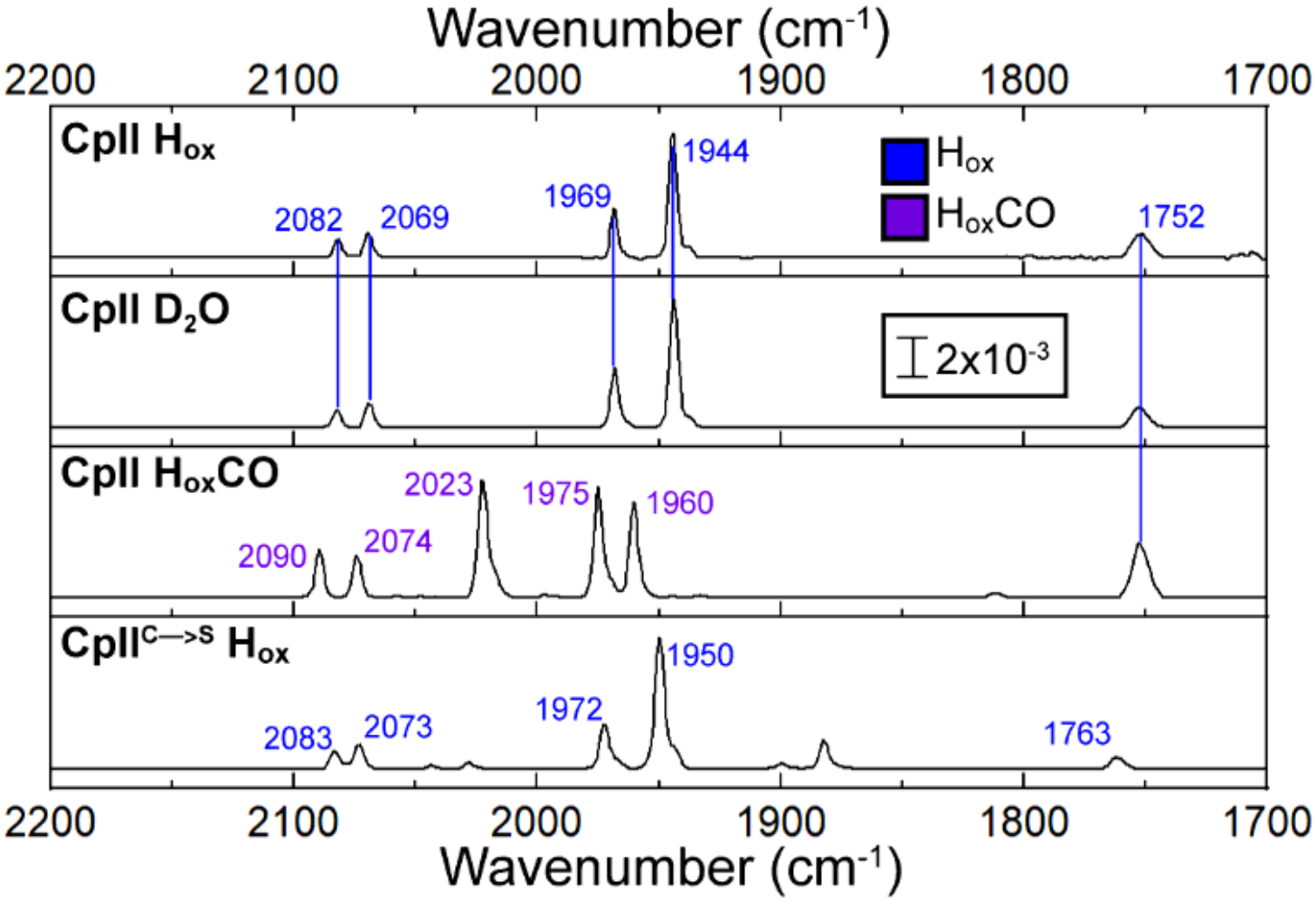

Figure 2

FTIR Spectra of Resting State and CO-inhibited CpII. FTIR collected at room temperature (295 K). CpII D2O does not display an isotope sensitive μ-CO band. CpII and CpIIC→S Hox were treated with 2 mM DCIP. CpII D2O was buffer-exchanged into pD 8.3 buffer, incubated overnight, and treated with 2 mM DCIP. CpII Hox-CO was sparged 1 min with 100% CO, then incubated for 1 h under CO headspace. All samples were in 50 mM Tris, pH/pD 8.3, 300 mM NaCl, and 5% glycerol with a concentration of 545 μM.

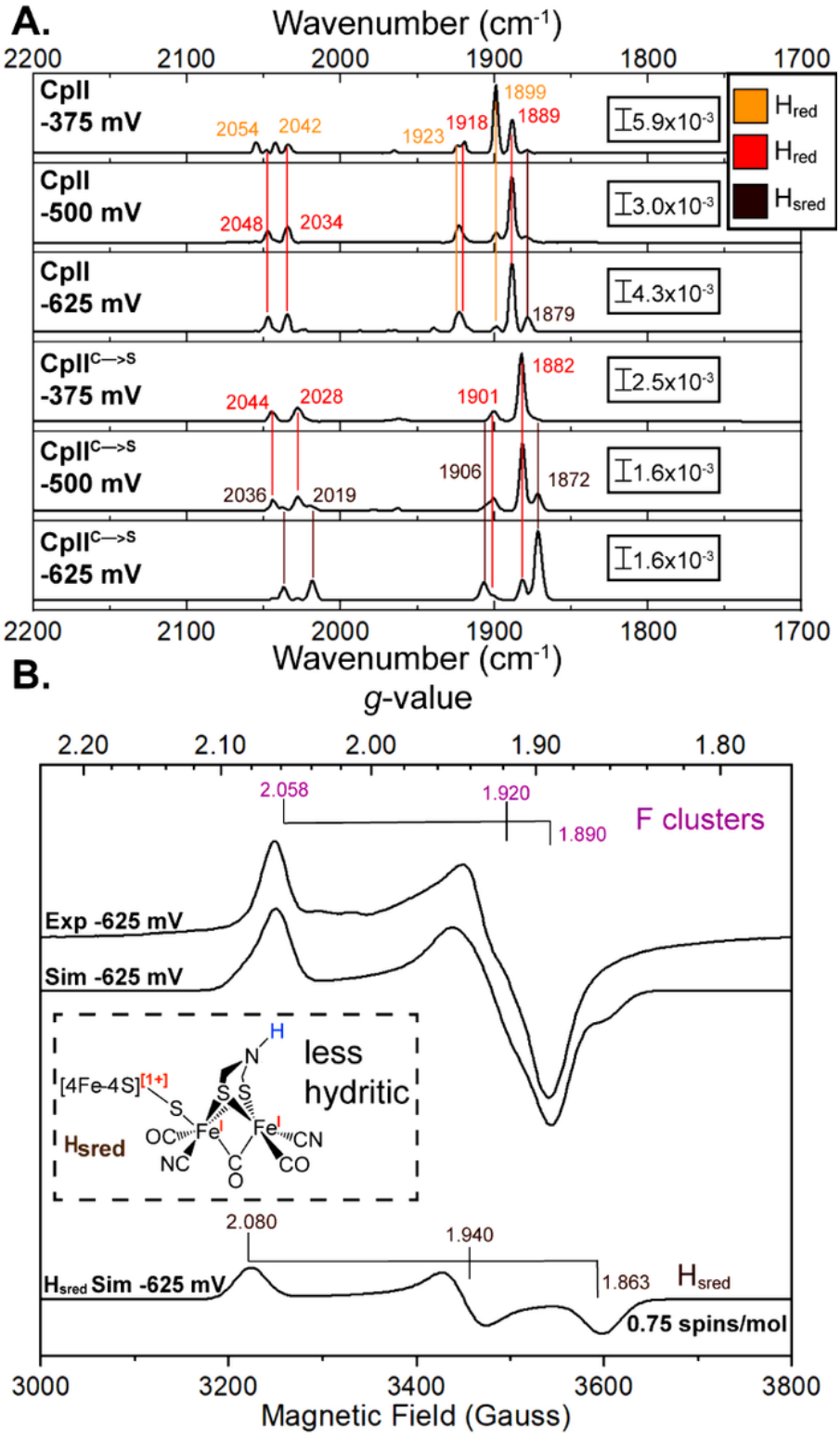

Figure 3

FTIR and EPR Spectra of Redox Poised CpII and CpIIC→S. A) FTIR spectra of CpII and CpIIC→S poised at -375, -500 and -625 mV (vs SHE). B) EPR spectrum of CpIIC→S poised at -625 mV (exp) with simulated spectrum (sim) consisting of F cluster (g = 2.058, 1.92, 1.89) and Hsred (g = 2.080, 1.940, 1.863) components. Below, the simulated Hsred component at -625 mV. EPR collected at 0.1 mW microwave power, 5 K sample temperature. EPR samples, 100 uM; FTIR samples, 545 µM. Buffer conditions were 50

mM MES pH 6, 300 mM NaCl, 5% glycerol, and 5 mM DT (-375 mV samples), 50 mM Tris pH 8.3, 300 mM NaCl, 5% glycerol, and 5 mM DT (-500 mV samples), 50 mM CHES pH 10.5, 300 mM NaCl, 5% glycerol, and 5 mM DT (-625 mV samples).

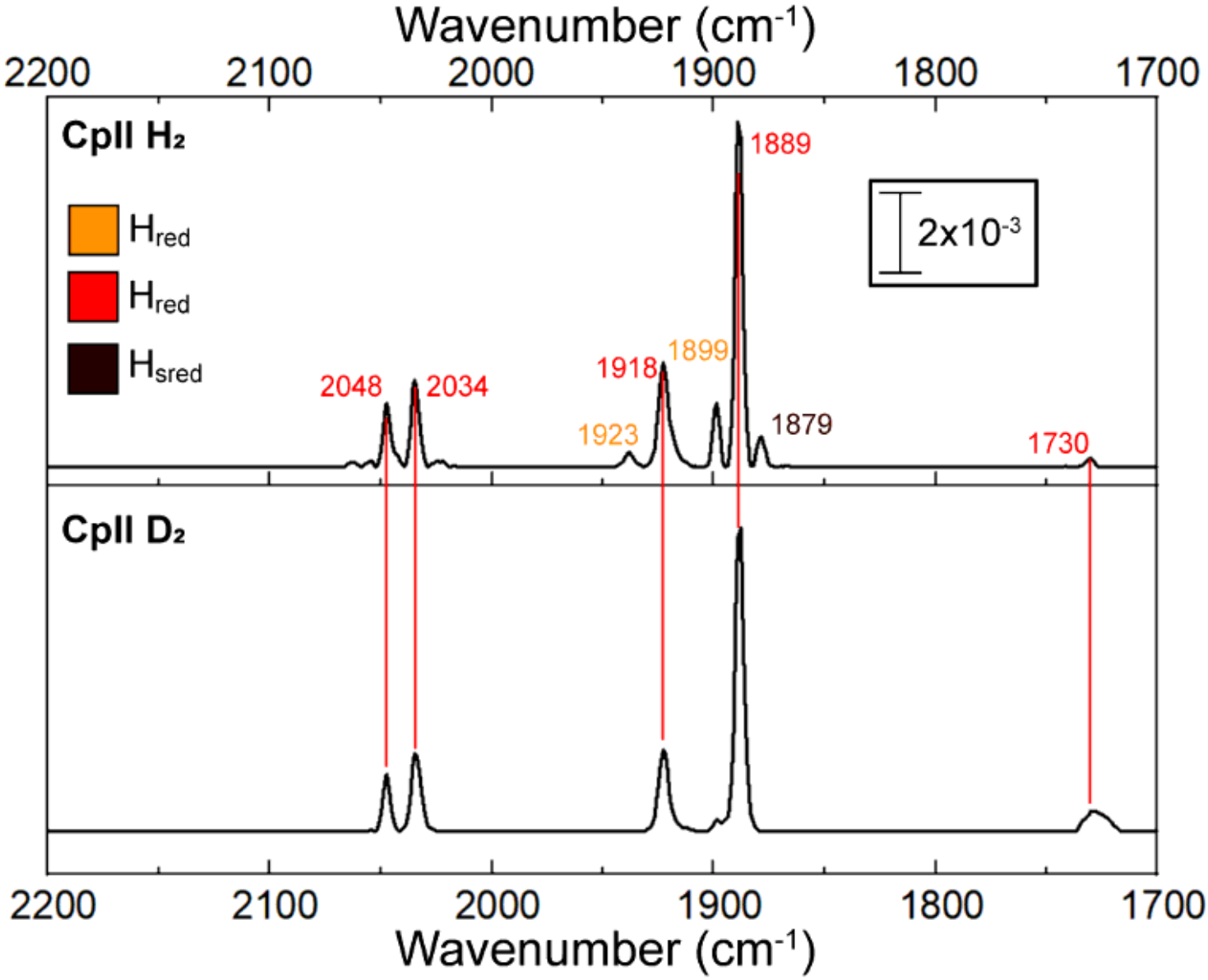

Figure 4

The FTIR Spectra of H2 and D2 Treated CpII. A) CpII was treated with 100% H2 (top panel) or exchanged into D2O buffer, incubated overnight, and treated with 100% D2 (bottom panel). Headspace exchange was carried out on a Schlenk line with 10 vacuum/sparge cycles, then incubation on ice for 1 h under 100% H2 or D2. The t-CO bands assigned to Hred (orange and red) and Hsred (brown). FTIR collected at 295 K. Samples were in 50 mM Tris, pH/pD 8.3, 300 mM NaCl buffer, and 5% glycerol with a concentration of 545 µM.

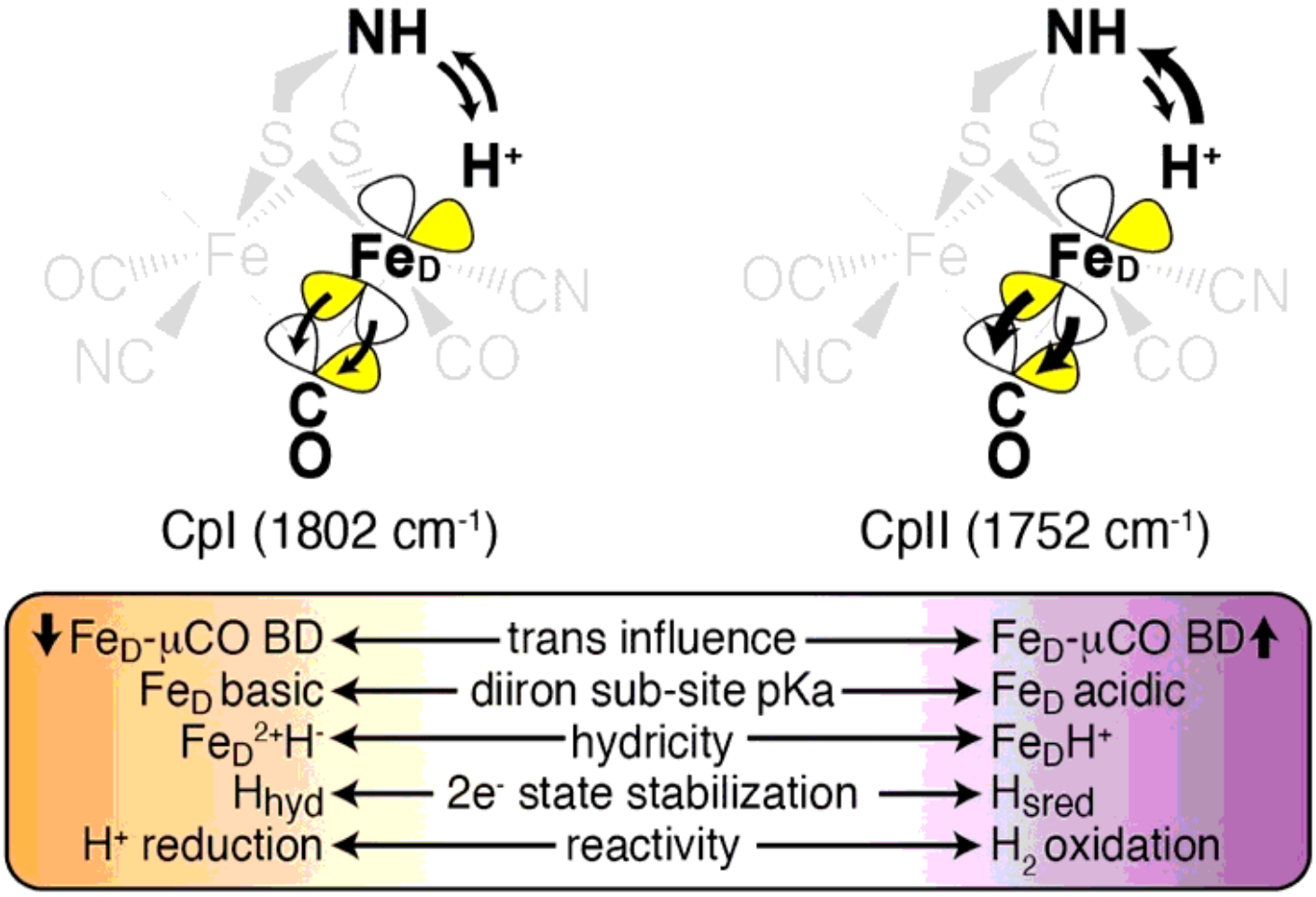

Figure 5

Electronic structure relationship to H cluster properties in [FeFe]-hydrogenases. The chart shows how the combination of bridging ligand trans-effect, metal site pKa, and hydricity of the H cluster manifest into differences in reactivity of [FeFe]-hydrogenases CpI and CpII. As a result of changes in metal site acidity, the pKa profile in CpII favors proton transfer from the H cluster to the relay to further support H2 oxidation. CpI values from Chen et al.56

Supplementary Files

This is a list of supplementary files associated with this preprint. Click to download.

- ArtzetalHydricityandReactivitySI.docx